

OpenFly: A Versatile Toolchain and Large-scale Benchmark for Aerial Vision-Language Navigation

Yunpeng Gao^{1,2*}, Chenhui Li^{1*}, Zhongrui You^{1,3*}, Junli Liu^{1,2*}, Zhen Li^{1,4*}, Peng Chen^{1,5}, Qizhi Chen^{1,6}, Zhonghan Tang^{1,7}, Liansheng Wang¹, Penghui Yang^{1,8}, Yiwen Tang^{1,2}, Yuhang Tang^{1,2}, Shuai Liang^{1,9}, Songyi Zhu¹, Ziqin Xiong^{1,4}, Yifei Su^{1,10}, Xinyi Ye¹, Jianan Li¹, Yan Ding¹, Dong Wang¹, Zhigang Wang^{1†}, Bin Zhao^{1,2†}, Xuelong Li^{1,11}

¹Shanghai AI Laboratory, ²Northwestern Polytechnical University,

³Beijing University of Posts and Telecommunications, ⁴Shanghai Jiao Tong University,

⁵The University of Hong Kong, ⁶Zhejiang University,

⁷University of Science and Technology of China,

⁸East China University of Science and Technology, ⁹Fudan University,

¹⁰Institute of Automation, Chinese Academy of Sciences, ¹¹TeleAI

*Equal Contribution, †Corresponding Author

<https://shailab-ipecc.github.io/openfly/>



Fig. 1: Overview of OpenFly. This work consists of an automatic toolchain for data generation, a large-scale aerial VLN dataset comprising 100K trajectories and instructions, and a keyframe-aware VLN model emphasizing key observations.

Abstract—Vision-Language Navigation (VLN) aims to guide agents through an environment by leveraging both language instructions and visual cues, playing a pivotal role in embodied AI. Indoor VLN has been extensively studied, whereas outdoor aerial VLN remains underexplored. The potential reason is that outdoor aerial view encompasses vast areas, making data collection more challenging, which results in a lack of benchmarks. To address this problem, we propose *OpenFly*, a platform comprising a versatile toolchain and large-scale benchmark for aerial VLN. Firstly, we develop a highly automated toolchain for data collection, enabling automatic point cloud acquisition, scene semantic segmentation, flight trajectory creation, and instruction generation. Secondly, based on the toolchain, we construct a large-scale aerial VLN dataset with 100k trajectories, covering diverse heights and lengths across 18 scenes. The corresponding

visual data are generated using various rendering engines and advanced techniques, including Unreal Engine, GTA V, Google Earth, and 3D Gaussian Splatting (3D GS). All data exhibit high visual quality. Particularly, 3D GS supports real-to-sim rendering, further enhancing the realism of the dataset. Thirdly, we propose *OpenFly-Agent*, a keyframe-aware VLN model, which takes language instructions, current observations, and historical keyframes as input, and outputs flight actions directly. Extensive analyses and experiments are conducted, showcasing the superiority of our *OpenFly* platform and *OpenFly-Agent*. The toolchain, dataset, and codes will be open-sourced.

I. INTRODUCTION

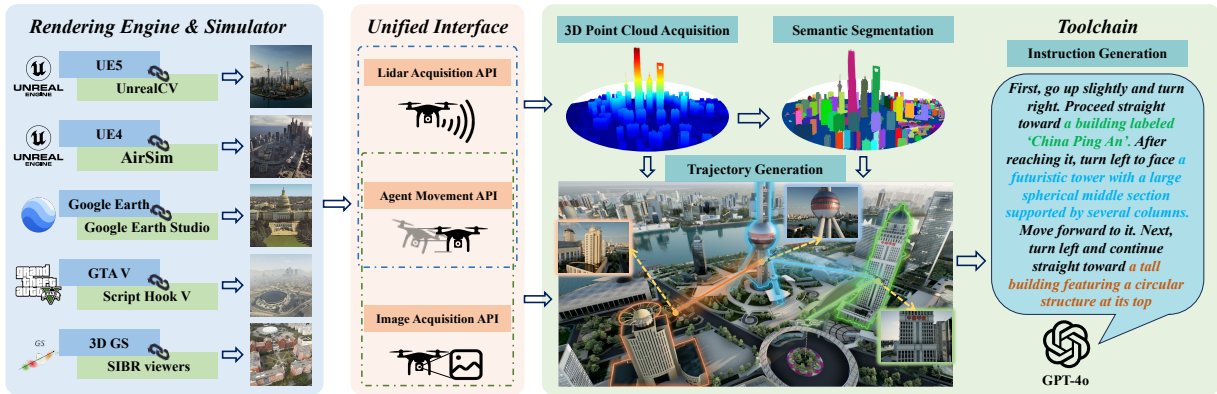


Fig. 2: Framework of the automatic data generation platform. Various rendering engines and simulators are first integrated, providing diverse high-quality scenes. Built on these, several interfaces and tools are developed, enabling automated generation of trajectories and instructions.

Embodied AI has drawn increasing research interest, where vision-language navigation (VLN) is a key task, aiming to navigate agents to a target location according to linguistic instructions and visual observations. Recently, many VLN datasets have been established, *e.g.*, TouchDown [7], REVERIE [36], R2R [1], RxR [25], CVDN [43], VLN-CE [23], and LANI [33], which significantly facilitate a series of VLN methods [30, 9, 38, 15, 17, 50, 49, 10, 52]. However, all these works focus on indoor or ground-based agents, overlooking unmanned aerial vehicles (UAVs) that play an important role in aerial photography, rescue operations, and cargo transportation.

Most recently, AerialVLN [29] and OpenUAV [45] have made significant strides by leveraging UAV simulators to bridge gaps in aerial VLN datasets, thus greatly advancing the development of this field. However, several challenges remain that need to be addressed:

- **Insufficient data diversity.** Existing methods rely on AirSim and Unreal Engine (UE) to control UAVs, limiting them to digital assets compatible with these platforms, reducing the diversity of available data and restricting the potential use of more photorealistic sources.
- **Inefficient data collection.** The process of generating trajectories relies on pilots operating UAVs in simulators, followed by manual annotation to create language instructions. The entire process is labor-intensive, time-consuming, and difficult to scale.
- **Inadequate data scale.** Current datasets for aerial VLN remain relatively small, with only around 10k trajectories, which is far behind embodied manipulation datasets. For example, Open X-Embodiment [35] has collected 1M episodes of manipulation data, which has significantly accelerated the development of vision-language-action (VLA) models.

To address these issues, we propose **OpenFly**, a comprehensive platform consisting of a versatile toolchain and a large-scale benchmark for the aerial VLN task. **To enhance data diversity**, the platform is established on various widely-used rendering engines and advanced techniques, *i.e.*, UE, GTA

V, Google Earth, and 3D Gaussian Splatting (3D GS). This enables us to utilize a wide range of assets as shown in Fig. 1. In particular, we use UAVs for automated patrols to capture numerous real-world images and integrate 3D GS technology into our platform, through which we reconstruct realistic 3D scenes. This empowers our platform to support a real-to-sim method, enhancing the realism of data. **To improve the efficiency of data collection**, we develop a versatile toolchain for automated aerial VLN data generation, as depicted in Fig. 2. Specifically, point cloud acquisition is first conducted to capture the 3D occupancy of a scene. Next, scene semantic segmentation is performed to identify and select landmarks as waypoints along the flight trajectories. Building on these tools, trajectory generation is then carried out, taking landmarks and point clouds as input, using predefined flight actions as basic units, and automatically searching for a collision-free trajectory. Finally, we feed the trajectories and corresponding UAV-egocentric images into a vision-language-model (VLM), *i.e.*, GPT-4o, to generate linguistic instructions. The entire pipeline is highly automated, reducing the reliance on UAV pilots and annotators. **To collect a large-scale dataset**, we meticulously collected 18 high-quality scenes, generating various trajectories of differing heights and lengths. Benefitting from our toolchain, we are able to quickly construct a dataset of **100k** samples, significantly larger than existing datasets.

Besides, we propose **OpenFly-Agent**, a keyframe-aware aerial VLN model trained on the OpenFly dataset. It is developed based on a VLA model OpenVLA [22] and incorporates an adaptive frame-level token-sampling mechanism to mitigate visual distraction caused by redundant historical observations. Note that this sampling mechanism is crucial for the visual encoding of aerial VLN, as UAVs fly quickly and observations change rapidly. Extensive experiments are conducted on the OpenFly dataset to evaluate numerous methods, establishing a comprehensive benchmark for the aerial VLN tasks.

Overall, our contributions can be summarized as follows:

- We build OpenFly on multiple rendering engines and develop a versatile toolchain, enabling the automatic genera-

tion of data with both great diversity and efficiency.

- We have constructed a novel aerial VLN benchmark comprising **100k** trajectories across 18 high-quality scenes. To the best of our knowledge, this is the largest aerial VLN benchmark to date.
- We propose OpenFly-Agent, a keyframe-aware VLN model. Extensive experiments demonstrate its superior performance compared to other methods.

II. RELATED WORKS

A. Simulators for Embodied AI

In recent years, many simulators related to embodied AI have been developed, *e.g.*, MuJoCo [44], Habitat [40], Pybullet [11], Matterport3D [6], OpenAI Gym [4], and Issac Gym [32]. They allow researchers to learn and validate algorithms in safe virtual environments, significantly advancing the development of embodied intelligence. However, most of them are designed for indoor robotic manipulation and navigation, making them unsuitable as simulators for aerial VLN tasks. Gazebo and AirSim [42] are two popular UAV simulators, while Gazebo suffers from low rendering quality. Combining AirSim and UE is a potential solution to construct aerial VLN scenes. Unfortunately, the official maintenance and updates for AirSim have been discontinued, resulting in a limited availability of compatible assets.

B. Vision-Language Navigation Datasets

Numerous datasets have been proposed to accelerate the VLN task. R2R [1] focuses on evaluating agents in unseen buildings and provides discrete navigation options. RxR [25] is a densely annotated VLN dataset, supporting multilingual instructions. TouchDown [7] and REVERIE [36] have each contributed a dataset from real-life environments, which requires a ground-based agent to follow instructions and find a target object. CVDN [43] presents a cooperative VLN dataset where agents can access the dialog history of human cooperation for inference. All the above datasets are graph-based where navigable points are predefined. LANI [33] and VLN-CE [23] propose the VLN task in continuous outdoor/indoor environments, enabling agents to move freely to any unobstructed point. Recently, a few works have tried to construct VLN datasets for aerial space. ANDH [12] establishes a dialogue-based aerial VLN dataset with bird-view images. CityNav [26] builds on the point cloud data from SensatUrban [18] and linguistic annotations from CityRefer [34], which requires a real-world 2D map to help locate specific landmarks in the instruction. AerialVLN [29] and OpenUAV [45] integrate AirSim and UE to create VLN scenes where pilots can control UAVs to generate various trajectories.

C. Vision-Language Navigation Methods

VLN methods require agents to understand and complete language instructions according to visual observations. In graph-based works [31, 47, 20, 13], agents move among predefined graph nodes. Recently, LLM-driven works [54, 53, 8]

use the reasoning ability of large language models to infer the next node. Although great progress has been achieved, these methods are not applicable in real unknown environments. In contrast, [39, 19, 24, 52] explore VLN in continuous environments for more realistic applications. More recently, a few works attempt to address the problem of aerial VLN based on UAVs, among which AerialVLN [29] proposes a lookahead guidance method to generate more reasonable ground-truth trajectories during training, and STMR [14] designs a matrix representation to improve the spatial reasoning of LLMs.

III. OPENFLY DATA GENERATION PLATFORM

In this section, we first describe several basic simulators and data resources, and then present the developed toolchain. The framework of the whole automatic data generation platform is illustrated in Fig. 2.

A. Basic Simulators and Data Resources

To collect a wide range of high-quality and realistic simulation data, we source the dataset from multiple rendering engines integrated with various simulators. Fig. 3 showcases several examples obtained from these rendering engines/techniques.

Unreal Engine + AirSim/UnrealCV. UE is a rendering engine capable of providing highly realistic interactive virtual environments. This platform has undergone five iterations, and each version features comprehensive and high-quality digital assets. In UE5, we meticulously select an official sample project named ‘City Sample’, which provides us with a large urban scene covering $25.3km^2$ and a smaller one covering $2.7km^2$. These scenes include a variety of assets such as buildings, streets, traffic lights, vehicles, and pedestrians. Besides, in UE4, we prepare six more high-quality scenes. Specifically, there are two large scenes showcasing the central urban areas of Shanghai and Guangzhou, covering areas of $30.88km^2$ and $58.56km^2$, respectively. The remaining four scenes are selected from AerialVLN [29]. They have smaller areas for totally about $26.64km^2$. These scenes encompass a wide range of architectural styles, including both Chinese and Western influences, as well as classical and modern designs. Additionally, the UE4 engine allows us to make adjustments in scene time to achieve different appearances of scenes under varying lighting conditions.

Airsim is an open-source simulator, which provides highly realistic simulated environments for UAVs and cars. We integrate the AirSim plugin into UE4 to obtain image data easily from the perspective of a UAV. Since AirSim does not support UE5 and stopped updating in 2022, we use the UnrealCV [51] plugin as an alternative for image acquisition in UE5. To realize a highly efficient data collection in simulated scenes, we modify the UE5 project to a C++ project, integrate the UnrealCV plugin, and package executables for multiple systems like Windows and Linux.

GTA V + Script Hook V. GTA V is an open-world game that is frequently used by computer vision researchers due to its highly realistic and dynamic virtual environment. The



Fig. 3: High-quality examples from different rendering engines and techniques, including several large cities such as Shanghai, Guangzhou, Los Angeles, Osaka, and etc., cover an area of over a hundred square kilometers in total. 3D GS provides five large campus scenes, further enhancing the diversity and realism of the data.

game features a meticulously crafted cityscape modeled after Los Angeles, encompassing various buildings and locations such as skyscrapers, gas stations, parks, and plazas, along with dynamic traffic flows and changes in lighting and shadows.

Script Hook V is a third-party library with the interface to GTA V’s native script functions. With the help of Script Hook V, we build an efficient and stable interface, which receives the pose information and returns accurate RGB images and lidar data. From the interface, we can control a virtual agent to collect the required data in an arbitrary pose and angle in the game.

Google Earth + Google Earth Studio. Google Earth is a virtual globe software, which builds a 3D earth model by integrating satellite imagery, aerial photographs, and Geographic Information System (GIS) data. From this engine, we select four urban scenes covering a total area of 53.60km^2 , *i.e.*, Berkeley, primarily consisting of traditional neighborhoods; Osaka, which features a mix of skyscrapers and historic buildings; and two areas with numerous landmarks: Washington, D.C., and St. Louis.

Google Earth Studio is a web-based animation and video production tool that allows us to create keyframes and set camera target points on the 2D and 3D maps of Google Earth. Using this functionality, we can quickly generate customized

tour videos by selecting specific routes and angles. In order to efficiently plan the route, we develop a function that automatically draws the flight trajectory in Google Earth Studio according to the selected area and predefined photo interval.

3D Gaussian Splatting + SIBR viewers. As a highly realistic reconstruction method, hierarchical 3D GS [21] employs a hierarchical training and display architecture, making it particularly suitable for rendering large-scale areas. Due to these features, we use this method to reconstruct and render multiple real scenes. We utilize the DJI M30T drone as the data collection device, which offers an automated oblique photography mode, enabling us to capture a large area of real-world data with minimal manpower. Practically, we gathered data from five campuses across three universities, which are East China University of Science and Technology, Northwestern Polytechnical University, and Shanghai Jiao Tong University (referred to as ECUST, NWPU, and SJTU). These campus scenes include various types and styles of landmarks, such as libraries, bell towers, waterways, lakes, playgrounds, construction sites, and lawns. The detailed information for the five campuses is presented in Table I. More details of the 3D GS data collection can be found in our supplementary material.

SIBR [3] viewers is a rendering tool designed for the 3D GS project, enabling visualization of a scene from arbitrary

TABLE I: Different 3D GS Scenes

Campus Name	Images	Area
ECUST (Fengxian Campus)	12008	1.06km ²
NWPU (Youyi Campus)	4648	0.8km ²
NWPU (Changan Campus)	23798	2.6km ²
SJTU (Minghang-East Zone)	20934	1.72km ²
SJTU (Minghang-West Zone)	9536	0.95km ²

viewpoints. The tool supports high-frame-rate scene rendering and provides various interactive modes for navigation. Building upon SIBR viewers, we developed an HTTP RESTful API that generates RGB images from arbitrary poses, simulating a UAV’s perspective.

B. Toolchain for Automatic Data Collection

To achieve automatic data generation, we integrate the above five simulators and design three unified interfaces, *i.e.*, the agent movement interface, the lidar data acquisition interface, and the image acquisition interface, allowing an agent to interact with any scene. Based on these interfaces, we further develop a toolchain, including 3D point cloud acquisition, scene semantic segmentation, automatic trajectory generation, and instruction generation. The framework of the whole data generation platform is illustrated in Fig. 2, with details of these interfaces and tools elaborated below.

Unified Interfaces. 1) Agent Movement Interface: We design a *CoorTrans* module, which implements a customized pose transformation matrix and scaling function to unify all simulator coordinate systems into a meter-based FLU (Front-Left-Up) convention. This interface enables precise agent positioning among regular scenes, point clouds, and scene segmentations, ensuring consistency and facilitating automatic trajectory generation. 2) Lidar Data Acquisition: For different simulators, point cloud data is acquired through different methods, including lidar sensor collection, depth map back-projection, and image feature matching. We develop a unified interface to integrate these methods and leverage the proposed *CoorTrans* module to align all data to the same FLU coordinate system. 3) Image Acquisition Interface: We integrate HTTP RESTful and TCP/IP protocols to form a unified image request interface, allowing image data to be obtained from any location with flexible resolutions and agent viewpoints.

3D Point Cloud Acquisition. For different simulators, we provide two methods to reconstruct the point cloud map of an entire scene. 1) Rasterized Sampling Reconstruction: For the UE5 + UnrealCV simulator, the MatrixCity [28] project offers a convenient rasterized sampling solution. We use the aforementioned lidar data acquisition interface to obtain the local point cloud at the sampling points. Since these data are already aligned within the same coordinate system, the point cloud map of the entire scene can be constructed by simply stitching local point clouds. For the UE4 + AirSim and GTA V simulators, we customize rasterized sampling points at appropriate resolutions, and perform sampling and recon-

struction using the agent movement and lidar data acquisition interfaces. 2) Image-based Sparse Reconstruction: In 3D GS, the scene reconstruction process begins with the open-source COLMAP [41] framework, which geneverlearates a sparse point cloud from input images. We directly export and use the point clouds obtained from this step.

Scene Semantic Segmentation. Vision-and-Language Navigation (VLN) requires meaningful landmarks as navigation targets. We perform semantic segmentation on four types of simulation scenes using the following three methods. 1) 3D Scene Understanding: A sequence of top-down views of the scene is captured in a rasterized format. We then use Octree graph [48] to extract 2D mask proposals, which are subsequently projected into the 3D point cloud space to generate semantic 3D segments. 2) Point Cloud Projection and Contour Extraction: We first acquire the point cloud of a scene, then project the voxelized point cloud onto a projection plane slightly above the ground. Using OpenCV, we perform a series of operations on the projected image, including binarization, erosion, and contour extraction, to obtain multiple instances along with their 2D coordinates. For each instance, the maximum height of the points within its neighborhood is used as the final height. This method provides a more computationally efficient yet coarser segmentation compared to the first approach, allowing users to choose based on their requirements. 3) Manual Annotation: When the point cloud quality of a scene is low or finer segmentation is required, we provide a method for annotating instances in the point cloud space by mouse clicks, based on ROS2 and RVIZ2. Users can annotate instances directly in the point cloud space using mouse clicks to define landmarks of interest for the task. This method is applicable to four simulators, *i.e.*, UE + UnrealCV, UE + Airsim, GTA V, and 3D GS.

Automatic Trajectory Generation. Leveraging the aforementioned point cloud map and segmentation tools, OpenFly can generate trajectories using the following two methods. 1) Path search based on customized action space: First, a global hash voxel map M_{global} and a bird’s eye view (BEV) occupancy map M_{bev} are constructed from the scene point cloud P . Second, the flight altitude is randomly selected within the user-defined height range, and landmarks that are not lower than the height threshold H_τ are chosen as targets. A starting point is selected within the distance range $[r, R]$ from the landmark, ensuring that it is not occupied in both M_{global} and M_{bev} . Then, a point on the line connecting the starting point and the landmark, which is close to the landmark and unoccupied in M_{bev} , is chosen as the endpoint. Third, A collision-free trajectory from the starting point to the endpoint is generated using the A* [16] pathfinding algorithm, where the granularity of exploration step size and direction can be adjusted according to the action space. Besides, by repeatedly selecting the endpoint as the new starting point, complex trajectories can be generated. Finally, utilizing OpenFly’s interface, images corresponding to the trajectory points can be obtained. 2) Path search based on grid: Google Map data does not allow image retrieval at arbitrary poses in the space.

Thus we rasterize a pre-selected area and collect images from each grid point in all possible orientations. Starting and ending points are chosen within the grid points to generate trajectories. Corresponding images for these trajectory points are then selected from the pre-collected image set.

Automatic Instruction Generation. Previous research has predominantly relied on manual annotation to generate trajectory instruction, which is not only costly but also limits the scalability of datasets. To address this issue, we propose a highly automated language instruction generation method based on VLMs, *e.g.*, GPT-4o. A straightforward method would be to submit all images to VLMs to analyze the trajectory and generate instructions. However, using all images introduces significant computational overhead and leads to information redundancy. For example, the ‘Forward’ action usually occupies a larger proportion of a flight trajectory, with ‘Turn Left/Turn Right’ or ‘Ascend/Descend’ actions taken when encountering key landmarks.

Based on the above findings, we split the complete trajectory into multiple sub-trajectories based on the occurrence of non-consistent actions, extracting key actions and images for processing and subsequent integration. Notably, slight angle adjustments often occur during flight to change the direction subtly, and a ‘slightly Turn Left/Right’ will be merged with subsequent ‘Forward’ actions. Specifically, suppose that the trajectory action sequence is [1, 1, 2, 1, 1, 2, 2, 1, 0], where 1, 2, and 0 denote ‘Forward’, ‘Turn Left’, and ‘Stop’, respectively. This trajectory would be split into four sub-trajectories, *i.e.*, [1, 1], [2, 1, 1], [2, 2], and [1, 0]. The second sub-trajectory involves ‘slightly turn left’ and ‘move forward’. We submit the action sequence and the last captured image of each sub-trajectory to a VLM to generate descriptions of both action and landmarks. The sub-instructions are obtained similar to the following format:

- ‘Move forward’ to ‘Landmark 1’.
- ‘Slightly turn left and move forward’ to ‘Landmark 2’.
- ‘Turn left’ towards ‘Landmark 3’.
- ‘Move forward’ to ‘Landmark 4’.

These sub-instructions are then processed by a VLM/LLM again, where they are integrated into coherent and complete instructions. The detailed prompt used for the VLM, along with the complete responses, is provided in the supplementary material.

C. Quality Control.

Data Filter. During data collection, it is inevitable that some damaged or low-quality data will be generated. We clean the data in the following situations. 1) We remove damaged images that are produced in generation or transmission. 2) We find that UAVs sometimes appear to pass through the tree models. Therefore, we exclude the trajectories where the altitude is lower than that of the trees. 3) We believe that extremely short or long trajectories are not conducive to model training. Thus, we remove these trajectories, specifically those with fewer than 2 or more than 150 actions.

Instruction Refinement. A known challenge of instruction generation is VLMs’ hallucinations. During the previous instruction generation process, sometimes the same landmark appears across several frames. This results in a VLM generating similar captions for the repeated observations of a landmark, increasing the complexity of the final instruction and introducing ambiguity due to duplication.

To mitigate this challenge, we utilize the NLTK library [2] to simplify the instruction by detecting and merging similar descriptions. Specifically, a syntactic parse tree is first constructed to extract all landmark captions using a rule-based approach. Then, a sentence-transformer model is employed to encode the extracted landmark captions into embedding vectors. Their similarities are computed with dot product, and high-similarity captions are then identified and replaced with referential pronouns (*e.g.*, “it,” “there,” *etc.*). For example, a generated instruction with redundant information is “... make a left turn toward a **medium-sized beige building marked by a signboard reading CHARLIE’S CHOCOLATE**. Continue heading straight, passing a **medium-sized gray building with a prominent rooftop billboard displaying Charlie’s Chocolate** ...”. After simplification, a more concise sentence is obtained, *i.e.*, “... make a left turn toward a **medium-sized beige building marked by a signboard reading CHARLIE’S CHOCOLATE**. Continue heading straight, passing it ...”, demonstrating the effectiveness of this post-processing technique.

At the same time, we built a data inspection platform to provide instructions, action sequences, and corresponding images to the examiners. If the instructions and trajectories align, they are considered qualified. We randomly select 3K samples from the entire dataset according to data distribution in Sec. V-A. After manually inspecting these samples, we find that the qualification rate reaches 91%.

IV. DATASET ANALYSIS

A. Overview

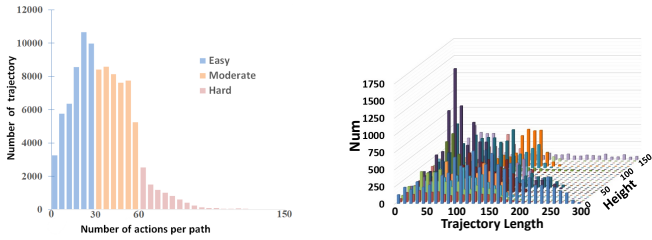
Using our toolchain, we collect 100k trajectories from 18 scenes, along with corresponding image sequences and language instructions. During the data generation process, we set a minimum motion step size of 3 meters to produce more granular trajectories. The details of our and previous VLN datasets are listed in Table II, from which we can see that our dataset features a significantly larger number of trajectories and a more extensive vocabulary, as well as greater environmental diversity. In contrast, our average trajectory length and instruction length are relatively short. This is intentional, as we believe” short- and medium-range instructions are actually more in line with the usage habits of human users. This might be more beneficial for the aerial VLN field.

B. Trajectory Analysis

In addition to a rich variety of scenes, we also strive for diversity in the difficulty level, length, and height of the trajectory data. Based on the number of actions in one trajectory, we classify trajectories with fewer than 30 actions

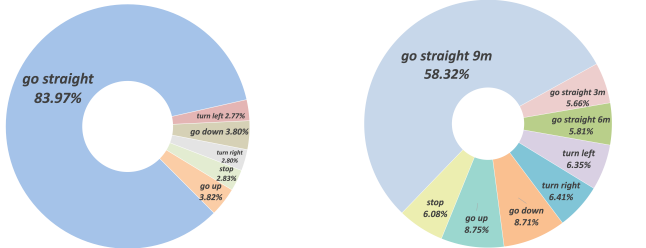
TABLE II: Comparison of different VLN datasets. Above the middle dividing line lies the ground-based datasets, while below is the aerial VLN datasets. N_{traj} : the number of total trajectories. N_{vocab} : vocabulary size. Path Len: the average length of trajectories, measured in meters. Intr Len: the average length of instructions. N_{act} : the average number of actions per trajectory.

Dataset	N_{traj}	N_{vocab}	Path Len.	Intr Len.	Action Space	N_{act}	Environment
R2R [1]	7189	3.1K	10.0	29	graph-based	5	Matterport3D
RxR [25]	13992	7.0K	14.9	129	graph-based	8	Matterport3D
REVERIE [36]	7000	1.6K	10.0	18	graph-based	5	Matterport3D
CVDN [43]	7415	4.4K	25.0	34	graph-based	7	Matterport3D
TouchDown [7]	9326	5.0K	313.9	90	graph-based	35	Google Street View
VLN-CE [23]	4475	4.3K	11.1	19	2 DoF	56	Matterport3D
LANI [33]	6000	2.3K	17.3	57	2 DoF	116	CHALET
ANDH [12]	6269	3.3K	144.7	89	3 DoF	7	xView
AerialVLN [29]	8446	4.5K	661.8	83	4 DoF	204	AirSim + UE
CityNav [26]	32637	6.6K	545	26	4 DoF	-	SensatUrban
OpenUAV [45]	12149	10.8K	255	104	6 DoF	264	AirSim + UE
Ours	100K	15.6K	99.1	59	4 DoF	35	AirSim + UE, GTA5 + Script Hook V, Google Earth Studio, 3D GS + SIBR viewers



(a) Difficulty level distribution.

(b) Length-height distribution.



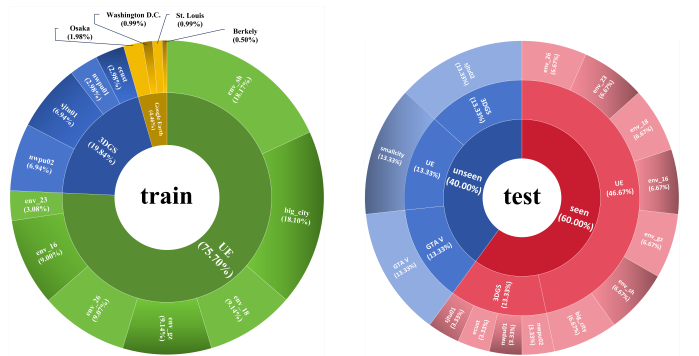
(c) Action distribution with 1 type of 'Forward'.

(d) Action distribution with 3 types of 'Forward'.

Fig. 4: Statistical analysis of trajectories.

as 'Easy', those with the number of actions ranging from 30 to 60 as 'Moderate', and those with more than 60 actions as 'Hard'. Fig. 4a shows the corresponding difficulty level distribution. Besides, compared with ground-based VLN, the aerial VLN task has more motion dimensions. Therefore, we set different trajectory lengths and flight heights to obtain rich data. Fig. 4b exhibits the distribution of these data, with their lengths ranging from 0 to 300 meters, and the heights ranging from 0 to 150 meters.

In the aerial VLN tasks of large-scale outdoor scenes, the proportion of moving forward is naturally higher than that of making adjustments in direction and altitude, as shown in



(a) Train set distribution.

(b) Test set distribution.

Fig. 5: The distribution of the data volume in different scenes under the Train and Test sets.

Fig. 4c. However, this highly unbalanced action distribution might cause the VLN model to overfit to the dominant action. To alleviate this problem, we divide the 'Forward' action into three granularities, *i.e.*, 3m, 6m, and 9m. In the ground-truth trajectories, three consecutive 'Forward' actions will be combined into one '9m Forward' action. At the end of a straight-moving trajectory, if the remaining distance is less than 9m, it will be combined into a '6m Forward' action, or remain as a '3m Forward' action. Fig. 4d presents the action distribution after this action merging process.

V. OPENFLY-AGENT

A. Dataset Split

Similar to previous works, we divide the dataset into three splits, *i.e.*, *Train*, *Test Seen*, *Test Unseen*. Detailed data distributions are shown in Fig. 5. For the *Train* split, 7 scenes under the UE rendering engine account for 75.7% of the total **100K** data, since UE provides the largest number of scenes, where

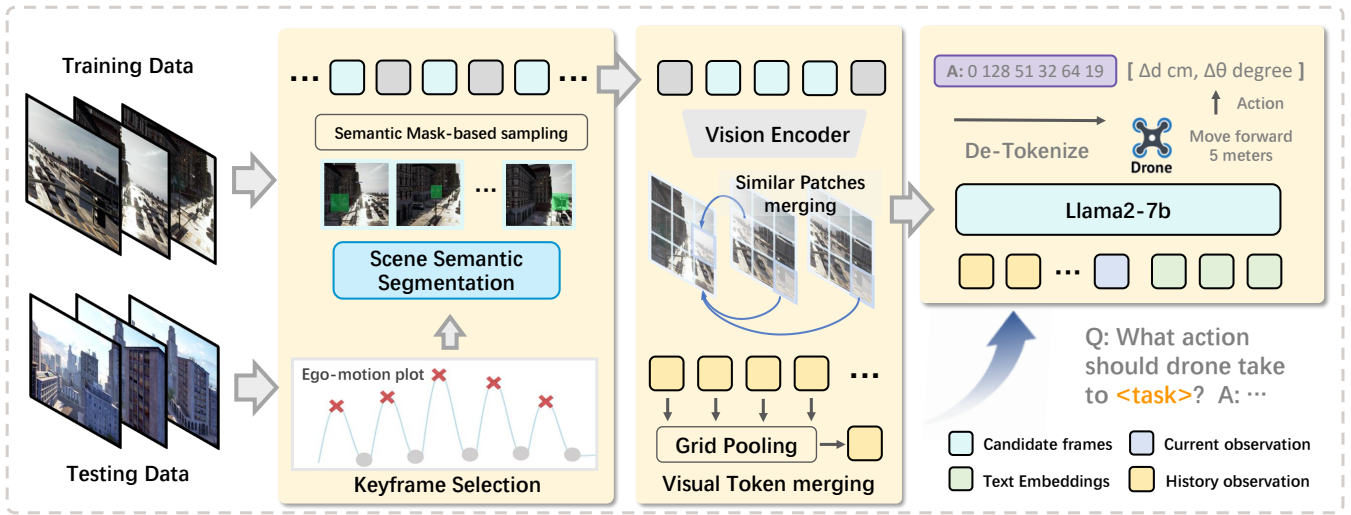


Fig. 6: The architecture of OpenFly-Agent. Keyframes at the time of action transitions are selected to extract crucial observations as the history, with corresponding visual tokens compressed to reduce the computational burden.

different amounts of trajectories are sampled according to the scenario area. The 4 scenes created by 3D GS are also the main part of the data, accounting for nearly 20% of the total amount. To ensure visual quality, we only collect data from a high-altitude perspective using Google Earth, which accounts for 4.46%. The detailed information of the *Test Seen* and *Test Unseen* splits are as follows:

- *Test Seen*: 1600 trajectories uniformly sampled from 11 previously seen UE and 3D GS scenarios.
- *Test Unseen*: 1400 trajectories uniformly generated from 3 unseen scenarios, *i.e.*, UE-smallcity, 3D GS-sjtu02, and a Los Angeles-like city in GTA V.

B. Problem Definition

In the aerial VLN task, a UAV is randomly positioned within a 3D environment with its initial pose defined as $P = [x, y, z, \phi, \theta, \psi]$. At each timestamp t , the UAV perceives the surrounding environment through an egocentric image as its observation. Guided by natural language instructions, the task involves predicting the next navigation action. Notably, the UAV can utilize either the current observations or the frames from all previous timestamps to make its prediction.

C. Model Architecture

As shown in Fig. 6, we take OpenVLA [22] as the baseline and design an end-to-end model for aerial VLN. In contrast, our model takes a sequence of images to indicate the observation instead of one image in the original OpenVLA. Moreover, to mitigate visual redundancy between adjacent video frames while maintaining key information, two strategies are proposed, *i.e.*, keyframe selection and visual token merging. First, a series of candidate keyframes are selected. Then, these keyframes are merged temporally before and after the vision encoder, resulting in a compact sequence of visual tokens. Finally, the action decoder discretizes the predicted tokens into

uniformly distributed bins, which are subsequently mapped to the 6 action types specific to drones.

1) *Keyframe Selection*: The length of contextual visual tokens is a major challenge for VLMs when processing videos. Many open-source VLMs use uniform frame sampling [5, 37, 46] to reduce calculation, but this strategy is not suitable for aerial VLN, since it may miss frames containing key landmarks. To address this issue, we adopt a heuristic method to identify keyframes by detecting the change point of the UAV’s movement. We notice that sudden changes in the UAV’s trajectory are often caused by the observation of landmarks, which can serve as cues to determine keyframes. Specifically, we use the movement of the drone over time to draw turning curves, and the frames near the peaks of the wave are selected as candidate keyframes. The resulting data is interpolated and smoothed, forming a wave-like curve that represents the UAV’s movement.

To further ensure the precision of training data, scene segmentation maps collected in Sec. III-A are used on selected frames to detect key landmarks. Frames containing landmarks are selected as keyframes, yielding reasonably accurate results. Note that each sudden change of actions, *e.g.*, from ‘Forward’ to ‘Turn Left’, will produce a set of keyframes. Consequently, we obtain several sets of keyframes for a long trajectory.

2) *Visual Token Merging*: To further reduce redundant information in keyframes, we design visual token merging, where the core concept is to recognize the similarity between image tokens. It compares adjacent keyframes to merge similar regions and maintains its simplicity by token compression.

For each set of candidate keyframes obtained in the previous selection process, a visual encoder maps each input image to multiple visual tokens, with each token representing the information of an image patch. Considering the potential inter-frame patch redundancy, we take a strategy that similar tokens in subsequent adjacent frames are periodically merged.

TABLE III: Comparison results on the test-seen split.

Method	Easy				Moderate				Hard				Total			
	NE↓	SR↑	OSR↑	SPL↑	NE↓	SR↑	OSR↑	SPL↑	NE↓	SR↑	OSR↑	SPL↑	NE↓	SR↑	OSR↑	SPL↑
Random	289m	0.9%	1.1%	0%	351m	1.3%	1.3%	0%	374m	0%	0%	0%	242m	0.7%	0.8%	0%
Seq2Seq[23]	201m	0.9%	21.2%	0.9%	190m	8.9%	19.2%	6.5%	192m	2.1%	10.1%	1.9%	194m	4.0%	16.8%	3.1%
CMA[23]	156m	1.2%	35.6%	1.6%	120m	11.2%	34.5%	8.4%	156m	4.6%	20.1%	5.3%	144m	5.7%	30.0%	5.1%
AerialVLN[29]	<u>148m</u>	1.5%	<u>40.2%</u>	2.6%	94m	<u>13.2%</u>	58.6%	<u>10.7%</u>	147m	5.4%	<u>23.6%</u>	<u>7.6%</u>	<u>130m</u>	6.6%	<u>40.8%</u>	<u>7.0%</u>
Navid[52]	151m	<u>11.2%</u>	28.9%	<u>4.5%</u>	138m	8.0%	21.3%	2.8%	<u>134m</u>	10.3%	21.3%	4.6%	142m	<u>9.9%</u>	24.3%	3.9%
Ours	111m	26.5%	55.6%	16.0%	<u>115m</u>	16.4%	<u>51.2%</u>	11.2%	120m	10.3%	29.6%	8.2%	115m	18.5%	50.9%	12.2%

Specifically, we select the first frame in a keyframe set as the reference, since it usually contains the crucial observation indicating the time for action transition. Then, we densely calculate the cosine similarities between each pair of visual tokens of the reference image and the subsequent image. Next, we merge the tokens with high similarity by averaging them. The unmerged tokens in the subsequent frame will be discarded. The merging operation is iteratively performed until the entire keyframe set has been traversed. Besides, we maintain a memory bank with a capacity of K images, which follows a first-in-first-out (FIFO) policy to retain the latest keyframes.

After the above process, M visual tokens $E = \{e_1, e_2, \dots, e_M\}$ are obtained for each set of keyframes. Since aerial VLN requires UAVs to perform long-distance flights based on instructions, we continue to carry out token compress to reduce the computational burden. The compressed visual tokens E_c are obtained through grid pooling [27]. Notably, we keep the visual tokens of the current frame uncompressed to capture the latest visual observation, as it contains the most important information for flight action prediction.

3) *Action Prediction*: Similar to [29, 26], 6 actions for UAVs are defined as {Forward, Turn Left, Turn Right, Move Up, Move Down, Stop} in this work. The units for ‘Move up’ and ‘Move down’ are 3 m, the units for ‘Turn Left’ and ‘Turn Right’ are 30 degrees. ‘Forward’ has three distinct units, namely 3 m, 6 m, and 9 m, respectively. For flight action prediction, each action type is discretized into multiple bins with one non-activate bin indicating that the current action is not activated. We map the model output to one of the bins for each action type, where the bin number corresponds to the amount of units in each action.

VI. EXPERIMENTS

A. Implementation and Training Details

The proposed OpenFly-Agent is composed of the Dino-SigCLIP (224 × 224 pixels) as a vision encoder and the pre-trained Llama-2 (7B) as a language model. The visual tokens extracted by Dino-SigLIP are aligned to the same dimension as text embeddings using a projection layer, and then fed into the Llama-2 model. The current frame during flight remains 256 tokens and all historical keyframes are compressed into 1 token. The capacity K of the history memory bank is set to 2 in our experiment. For action prediction, the last 256

tokens in the vocabulary are used as special tokens for action representation.

B. Evaluation Metrics

Four standard metrics in VLN tasks are adopted to evaluate different methods, *i.e.*, navigation error (NE), success rate (SR), oracle success rate (OSR), and success weighted by path length (SPL). NE measures the average deviation between the UAV’s final stopping point and the ground-truth destination. SR calculates the proportion of successful tasks, where a task is considered successful if the UAV stops within 20 m of the target. In OSR, if any point on the trajectory is within 20 m of the target, the task can be considered successful. SPL calculates the success rate weighted by the ratio of the ground-truth path length to the actually-executed path length.

C. Results

1) *Quantitative results*: We test the proposed OpenFly-Agent on the test-seen and test-unseen splits and differentiate among easy, moderate, and hard difficulty levels. Multiple VLN methods are compared with ours, where ‘Random’ means an agent randomly selects one action to execute until the ‘stop’ action is chosen, Seq2Seq [23] adopts a simple recurrent model for action sequence prediction, CMA [23] uses a bi-directional LSTM to implement cross-modal attention between instructions and images, AerialVLN [29] combines CMA and a look-ahead guidance strategy to enhance robustness. Navid [52] leverages the strong ability of VLMs and develops a video-based architecture, achieving impressive results in indoor VLN.

Table. III shows quantitative results on the test-seen split. Seq2Seq, CMA, and AerialVLN achieve limited success rates. Counterintuitively, they perform worse on easy samples. We find that their OSR is not low while they are difficult to stop at a short-range distance. In contrast, Navid obtains better results, demonstrating the great potential of VLMs in aerial VLN. Our OpenFly-Agent achieves the best performance for its strong VLM backbone and the proposed strategies, while there is still much room for improvement. Table. IV presents quantitative results on the test-unseen split, illustrating the generalization capabilities of these VLN methods. Similarly, our method achieves better performance, exhibiting a certain degree of robustness. However, all methods are significantly degraded, which indicates models with greater generalization are urgently needed to be developed.

TABLE IV: Comparison results on the test-unseen split.

Method	Easy				Moderate				Hard				Total			
	NE↓	SR↑	OSR↑	SPL↑												
Random	321m	0.1%	0.2%	0%	231m	0.1%	0.1%	0%	371m	0%	0%	0%	301m	0.1%	0.1%	0%
Seq2Seq[23]	298m	0.1%	1.1%	0.8%	286m	0.2%	7.6%	0.4%	291m	0.1%	0.9%	0.6%	291m	0.1%	3.2%	0.6%
CMA[23]	278m	1.1%	9.1%	1.2%	234m	0.9%	9.8%	0.6%	293m	0.1%	1.0%	0.4%	268m	0.7%	6.6%	0.7%
AerialVLN[29]	263m	3.2%	21.4%	3.2%	<u>225m</u>	<u>1.3%</u>	<u>19.8%</u>	<u>1.2%</u>	195m	<u>2.5%</u>	18.2%	<u>2.1%</u>	<u>227m</u>	2.3%	19.8%	2.2%
Navid[52]	<u>259m</u>	<u>5.2%</u>	<u>26.8%</u>	<u>4.9%</u>	278m	1.2%	12.5%	1.1%	<u>193m</u>	2.2%	<u>17.8%</u>	1.9%	231m	4.2%	<u>27.0%</u>	3.5%
Ours	219m	9.1%	29.8%	7.0%	209m	2.3%	36.4%	1.4%	170m	4.3%	16.5%	2.6%	198m	5.1%	27.3%	3.5%

TABLE V: Ablation study on the test-seen split. ‘KS’ and ‘VTM’ denote keyframe selection and visual token merging, respectively.

Method	NE↓	SR↑	OSR↑	SPL↑
OpenVLA[22] (baseline)	196m	3.6%	12.4%	1.9%
History + VTM	215m	12.7%	39.6%	6.4%
KS	275m	6.2%	24.1%	5.6%
KS + VTM	115m	18.5%	50.9%	12.2%

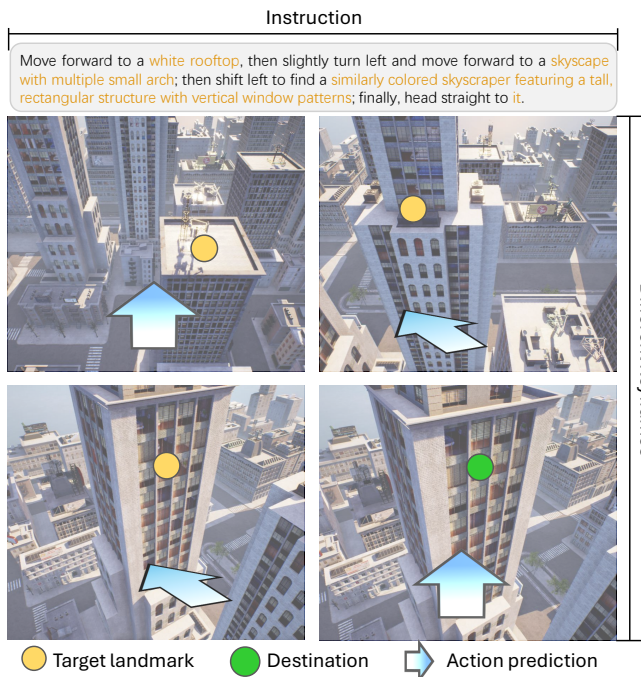


Fig. 7: Illustration of an aerial VLN trajectory generated by OpenFly-Agent, which successfully predicts actions following the instruction when encountering landmarks.

2) *Qualitative results*: Fig. 7 presents a qualitative result, where our OpenFly-Agent successfully navigates to the destination according to the instruction. It presents a powerful capability in perceiving environments and aligning observations with complex instructions. In addition, Fig. 8 shows two failure cases, where our model fails to identify the landmark or output actions with proper amplitudes.

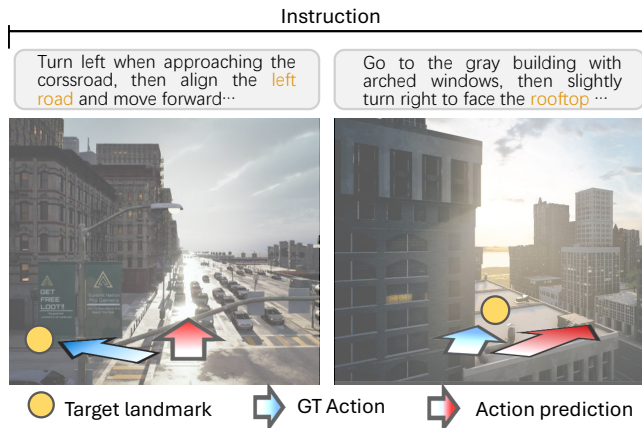


Fig. 8: Illustration of failure cases. Sometimes our model may misclassify key landmarks or output wrong actions.

D. Ablation Study

Ablation studies are conducted to evaluate the contribution of the keyframe selection and visual token merging in OpenFly-Agent. Table. V shows the results, where OpenVLA [22] is our baseline. Using only the current frame as an observation makes OpenVLA perform poorly in the aerial VLN task. From ‘History + VTM’ we can see that historical frames significantly improve the success rate. The keyframe selection strategy further increases the SR from 12.7% to 18.5%, demonstrating the effectiveness of key observations. Besides, the comparison between ‘KS’ and ‘KS + VTM’ indicates the great effect of our visual token merging strategy.

VII. LIMITATIONS AND FUTURE WORK

The proposed OpenFly platform incorporates various rendering engines/techniques to provide high-quality scenes. Specifically, this is the first attempt to use 3D GS reconstructed scenes to support real-to-sim training and testing, while in the reconstruction of large-scale areas, a few visual artifacts are inevitably present. Future work will focus on exploring more effective reconstruction methods to enhance realism in large-scale scenes. Besides, the proposed OpenFly-Agent is built upon the large VLN model architecture, which is not practical for real-time deployment on UAVs. To address this, future research should focus on developing more efficient architectures and effective quantization techniques.

VIII. CONCLUSION

In this work, we present OpenFly, a platform designed for large-scale data collection in aerial Vision-and-Language Navigation (VLN). OpenFly integrates multiple rendering engines and advanced real-to-sim techniques for data generation, enabling efficient collection of diverse, high-quality aerial VLN data. The resulting large-scale dataset comprises 100k trajectories across 18 distinct scenes, spanning a wide range of altitudes and difficulty levels, which is significantly superior than existing ones. Furthermore, we propose OpenFly-Agent, a keyframe-aware aerial navigation model capable of directly predicting flight actions based on observations and language instructions. Extensive experiments validate the effectiveness of the proposed method, and establishing a comprehensive benchmark for future advancements in aerial navigation.

REFERENCES

- [1] Peter Anderson, Qi Wu, Damien Teney, Jake Bruce, Mark Johnson, Niko Sünderhauf, Ian D. Reid, Stephen Gould, and Anton van den Hengel. Vision-and-language navigation: Interpreting visually-grounded navigation instructions in real environments. In *IEEE Conference on Computer Vision and Pattern Recognition*, 2018. 2, 3, 7
- [2] Steven Bird. Nltk: the natural language toolkit. In *Proceedings of the COLING/ACL 2006 Interactive Presentation Sessions*, pages 69–72, 2006. 6
- [3] Sebastien Bonopera, Peter Hedman, Jerome Esnault, Sidhant Prakash, Simon Rodriguez, Theo Thonat, Mehdi Benadel, Gaurav Chaurasia, Julien Philip, and George Drettakis. sibr: A system for image based rendering, 2020. 4
- [4] Greg Brockman, Vicki Cheung, Ludwig Pettersson, Jonas Schneider, John Schulman, Jie Tang, and Wojciech Zaremba. Openai gym. *CoRR*, abs/1606.01540, 2016. 3
- [5] Shyamal Buch, Cristóbal Eyzaguirre, Adrien Gaidon, Jiajun Wu, Li Fei-Fei, and Juan Carlos Niebles. Re-visiting the” video” in video-language understanding. In *Proceedings of the IEEE/CVF conference on computer vision and pattern recognition*, pages 2917–2927, 2022. 8
- [6] Angel X. Chang, Angela Dai, Thomas A. Funkhouser, Maciej Halber, Matthias Nießner, Manolis Savva, Shuran Song, Andy Zeng, and Yinda Zhang. Matterport3d: Learning from RGB-D data in indoor environments. In *2017 International Conference on 3D Vision, 3DV 2017, Qingdao, China, October 10-12, 2017*, pages 667–676, 2017. 3
- [7] Howard Chen, Alane Suhr, Dipendra Misra, Noah Snaveley, and Yoav Artzi. TOUCHDOWN: natural language navigation and spatial reasoning in visual street environments. In *IEEE Conference on Computer Vision and Pattern Recognition*, 2019. 2, 3, 7
- [8] Jiaqi Chen, Bingqian Lin, Ran Xu, Zhenhua Chai, Xiaodan Liang, and Kwan-Yee Kenneth Wong. Mapgpt: Map-guided prompting with adaptive path planning for vision-and-language navigation. In *Proceedings of the 62nd Annual Meeting of the Association for Computational Linguistics (Volume 1: Long Papers), ACL 2024, Bangkok, Thailand, August 11-16, 2024*, pages 9796–9810, 2024. 3
- [9] Kevin Chen, Junshen K Chen, Jo Chuang, Marynel Vázquez, and Silvio Savarese. Topological planning with transformers for vision-and-language navigation. In *Proceedings of the IEEE/CVF Conference on Computer Vision and Pattern Recognition*, pages 11276–11286, 2021. 2
- [10] Peihao Chen, Dongyu Ji, Kunyang Lin, Runhao Zeng, Thomas H Li, Mingkui Tan, and Chuang Gan. Weakly-supervised multi-granularity map learning for vision-and-language navigation. *arXiv preprint arXiv:2210.07506*, 2022. 2
- [11] Erwin Coumans and Yunfei Bai. Pybullet, a python module for physics simulation for games, robotics and machine learning, 2016–2021. 3
- [12] Yue Fan, Winson X. Chen, Tongzhou Jiang, Chunni Zhou, Yi Zhang, and Xin Wang. Aerial vision-and-dialog navigation. *ArXiv*, abs/2205.12219, 2022. 3, 7
- [13] Tsu-Jui Fu, Xin Eric Wang, Matthew F. Peterson, Scott T. Grafton, Miguel P. Eckstein, and William Yang Wang. Counterfactual Vision-and-Language Navigation via Adversarial Path Sampler, page 71–86. 2020. 3
- [14] Yunpeng Gao, Zhigang Wang, Linglin Jing, Dong Wang, Xuelong Li, and Bin Zhao. Aerial vision-and-language navigation via semantic-topo-metric representation guided LLM reasoning. *CoRR*, abs/2410.08500, 2024. 3
- [15] Georgios Georgakis, Karl Schmeckpeper, Karan Wanchoo, Soham Dan, Eleni Miltsakaki, Dan Roth, and Kostas Daniilidis. Cross-modal map learning for vision and language navigation. In *Proceedings of the IEEE/CVF Conference on Computer Vision and Pattern Recognition*, pages 15460–15470, 2022. 2
- [16] Peter E Hart, Nils J Nilsson, and Bertram Raphael. A formal basis for the heuristic determination of minimum cost paths. *IEEE transactions on Systems Science and Cybernetics*, 4(2):100–107, 1968. 5
- [17] Yicong Hong, Zun Wang, Qi Wu, and Stephen Gould. Bridging the gap between learning in discrete and continuous environments for vision-and-language navigation. In *Proceedings of the IEEE/CVF Conference on Computer Vision and Pattern Recognition*, pages 15439–15449, 2022. 2
- [18] Qingyong Hu, Bo Yang, Sheikh Khalid, Wen Xiao, Niki Trigoni, and Andrew Markham. Sensaturban: Learning semantics from urban-scale photogrammetric point clouds. *Int. J. Comput. Vis.*, 130(2):316–343, 2022. 3
- [19] MuhammadZubair Irshad, NiluthpolChowdhury Mithun, Zachary Seymour, Han-Pang Chiu, Supun Samarasekera, and Rakesh Kumar. Sasra: Semantically-aware spatio-temporal reasoning agent for vision-and-

- language navigation in continuous environments. *arXiv: Robotics, arXiv: Robotics*, 2021. 3
- [20] Liyiming Ke, Xiujun Li, Yonatan Bisk, Ari Holtzman, Zhe Gan, Jingjing Liu, Jianfeng Gao, Yejin Choi, and Siddhartha Srinivasa. Tactical rewind: Self-correction via backtracking in vision-and-language navigation. In *2019 IEEE/CVF Conference on Computer Vision and Pattern Recognition (CVPR)*, 2019. 3
- [21] Bernhard Kerbl, Andreas Meuleman, Georgios Kopanas, Michael Wimmer, Alexandre Lanvin, and George Drettakis. A hierarchical 3d gaussian representation for real-time rendering of very large datasets. *ACM Transactions on Graphics (TOG)*, 43(4):1–15, 2024. 4
- [22] Moo Jin Kim, Karl Pertsch, Siddharth Karamcheti, Ted Xiao, Ashwin Balakrishna, Suraj Nair, Rafael Rafailov, Ethan Foster, Grace Lam, Pannag Sanketi, Quan Vuong, Thomas Kollar, Benjamin Burchfiel, Russ Tedrake, Dorsa Sadigh, Sergey Levine, Percy Liang, and Chelsea Finn. Openvla: An open-source vision-language-action model. *arXiv preprint arXiv:2406.09246*, 2024. 2, 8, 10
- [23] Jacob Krantz, Erik Wijmans, Arjun Majumdar, Dhruv Batra, and Stefan Lee. Beyond the nav-graph: Vision-and-language navigation in continuous environments. In *Computer Vision - ECCV 2020 - 16th European Conference, Glasgow, 2020*. 2, 3, 7, 9, 10
- [24] Jacob Krantz, Aaron Gokaslan, Dhruv Batra, Stefan Lee, and Oleksandr Maksymets. Waypoint models for instruction-guided navigation in continuous environments. In *2021 IEEE/CVF International Conference on Computer Vision (ICCV)*, 2021. 3
- [25] Alexander Ku, Peter Anderson, Roma Patel, Eugene Ie, and Jason Baldridge. Room-across-room: Multilingual vision-and-language navigation with dense spatiotemporal grounding. In *Proceedings of the 2020 Conference on Empirical Methods in Natural Language Processing*, 2020. 2, 3, 7
- [26] Jungdae Lee, Taiki Miyanishi, Shuhei Kurita, Koya Sakamoto, Daichi Azuma, Yutaka Matsuo, and Nakamasa Inoue. Citynav: Language-goal aerial navigation dataset with geographic information. *CoRR*, abs/2406.14240, 2024. 3, 7, 9
- [27] Yanwei Li, Chengyao Wang, and Jiaya Jia. Llama-vid: An image is worth 2 tokens in large language models. In *Computer Vision - ECCV 2024 - 18th European Conference, Milan, Italy, September 29-October 4, 2024, Proceedings, Part XLVI*, volume 15104, pages 323–340, 2024. 9
- [28] Yixuan Li, Lihan Jiang, Linning Xu, Yuanbo Xiangli, Zhenzhi Wang, Dahua Lin, and Bo Dai. Matrixcity: A large-scale city dataset for city-scale neural rendering and beyond. In *Proceedings of the IEEE/CVF International Conference on Computer Vision*, pages 3205–3215, 2023. 5
- [29] Shubo Liu, Hongsheng Zhang, Yuankai Qi, Peng Wang, Yanning Zhang, and Qi Wu. Aerialvln: Vision-and-language navigation for uavs. In *IEEE/CVF International Conference on Computer Vision, ICCV 2023, Paris, France, October 1-6, 2023*, pages 15338–15348, 2023. 2, 3, 7, 9, 10
- [30] Yuxing Long, Wenzhe Cai, Hongcheng Wang, Guanqi Zhan, and Hao Dong. Instructnav: Zero-shot system for generic instruction navigation in unexplored environment. *arXiv preprint arXiv:2406.04882*, 2024. 2
- [31] Chih-Yao Ma, Jing Lu, Zuxuan Wu, Ghassan AlRegib, Zsolt Kira, Richard Socher, and Caiming Xiong. Self-monitoring navigation agent via auxiliary progress estimation. *arXiv: Artificial Intelligence, arXiv: Artificial Intelligence*, 2019. 3
- [32] Viktor Makoviychuk, Lukasz Wawrzyniak, Yunrong Guo, Michelle Lu, Kier Storey, Miles Macklin, David Hoeller, Nikita Rudin, Arthur Allshire, Ankur Handa, and Gavriel State. Isaac gym: High performance gpu-based physics simulation for robot learning. *CoRR*, abs/2108.10470, 2021. 3
- [33] Dipendra Kumar Misra, Andrew Bennett, Valts Blukis, Eyvind Niklasson, Max Shatkhin, and Yoav Artzi. Mapping instructions to actions in 3d environments with visual goal prediction. In *Proceedings of the 2018 Conference on Empirical Methods in Natural Language Processing, Brussels, 2018*. 2, 3, 7
- [34] Taiki Miyanishi, Fumiya Kitamori, Shuhei Kurita, Jungdae Lee, Motoaki Kawanabe, and Nakamasa Inoue. Cityrefer: Geography-aware 3d visual grounding dataset on city-scale point cloud data. In *Advances in Neural Information Processing Systems 36: Annual Conference on Neural Information Processing Systems 2023, NeurIPS 2023, New Orleans, LA, USA, December 10 - 16, 2023*. 3
- [35] Abby O’Neill, Abdul Rehman, and et al. Open x-embodiment: Robotic learning datasets and RT-X models : Open x-embodiment collaboration. In *IEEE International Conference on Robotics and Automation, ICRA 2024, Yokohama, Japan, May 13-17, 2024*, pages 6892–6903, 2024. 2
- [36] Yuankai Qi, Qi Wu, Peter Anderson, Xin Wang, William Yang Wang, Chunhua Shen, and Anton van den Hengel. REVERIE: remote embodied visual referring expression in real indoor environments. In *IEEE/CVF Conference on Computer Vision and Pattern Recognition, CVPR, 2020*. 2, 3, 7
- [37] Kanchana Ranasinghe, Xiang Li, Kumara Kahatapitiya, and Michael S Ryoo. Understanding long videos in one multimodal language model pass. *arXiv preprint arXiv:2403.16998*, 2024. 8
- [38] Sonia Raychaudhuri, Saim Wani, Shivansh Patel, Unnat Jain, and Angel X Chang. Language-aligned waypoint (law) supervision for vision-and-language navigation in continuous environments. *arXiv preprint arXiv:2109.15207*, 2021. 2
- [39] Sonia Raychaudhuri, Saim Wani, Shivansh Patel, Unnat Jain, and Angel X. Chang. Language-aligned waypoint (law) supervision for vision-and-language navigation in

- continuous environments. *Empirical Methods in Natural Language Processing*, *Empirical Methods in Natural Language Processing*, 2021. 3
- [40] Manolis Savva, Abhishek Kadian, Oleksandr Maksymets, Yili Zhao, Erik Wijmans, Bhavana Jain, Julian Straub, Jia Liu, Vladlen Koltun, Jitendra Malik, Devi Parikh, and Dhruv Batra. Habitat: A platform for embodied AI research. *CoRR*, abs/1904.01201, 2019. 3
- [41] Johannes Lutz Schönberger and Jan-Michael Frahm. Structure-from-motion revisited. In *Conference on Computer Vision and Pattern Recognition (CVPR)*, 2016. 5
- [42] Shital Shah, Debadeepta Dey, Chris Lovett, and Ashish Kapoor. Airsim: High-fidelity visual and physical simulation for autonomous vehicles. *CoRR*, abs/1705.05065, 2017. 3
- [43] Jesse Thomason, Michael Murray, Maya Cakmak, and Luke Zettlemoyer. Vision-and-dialog navigation. In *3rd Annual Conference on Robot Learning, CoRL 2019, Osaka, Japan, October 30 - November 1, 2019, Proceedings*, volume 100 of *Proceedings of Machine Learning Research*, pages 394–406, 2019. 2, 3, 7
- [44] Emanuel Todorov, Tom Erez, and Yuval Tassa. Mujoco: A physics engine for model-based control. In *2012 IEEE/RSJ International Conference on Intelligent Robots and Systems*, pages 5026–5033, 2012. 3
- [45] Xiangyu Wang, Donglin Yang, Ziqin Wang, Hohin Kwan, Jinyu Chen, Wenjun Wu, Hongsheng Li, Yue Liao, and Si Liu. Towards realistic UAV vision-language navigation: Platform, benchmark, and methodology. *CoRR*, abs/2410.07087, 2024. 2, 3, 7
- [46] Xiaohan Wang, Yuhui Zhang, Orr Zohar, and Serena Yeung-Levy. Videoagent: Long-form video understanding with large language model as agent. In *European Conference on Computer Vision*, pages 58–76. Springer, 2025. 8
- [47] Xin Wang, Qiuyuan Huang, Asli Celikyilmaz, Jianfeng Gao, Dinghan Shen, Yuan-Fang Wang, William Yang Wang, and Lei Zhang. Reinforced cross-modal matching and self-supervised imitation learning for vision-language navigation. In *2019 IEEE/CVF Conference on Computer Vision and Pattern Recognition (CVPR)*, 2019. 3
- [48] Zhigang Wang, Yifei Su, Chenhui Li, Dong Wang, Yan Huang, Bin Zhao, and Xuelong Li. Open-vocabulary octree-graph for 3d scene understanding. *CoRR*, abs/2411.16253, 2024. 5
- [49] Zihan Wang, Xiangyang Li, Jiahao Yang, Yeqi Liu, and Shuqiang Jiang. Gridmm: Grid memory map for vision-and-language navigation. In *Proceedings of the IEEE/CVF International Conference on Computer Vision*, pages 15625–15636, 2023. 2
- [50] Zihan Wang, Xiangyang Li, Jiahao Yang, Yeqi Liu, and Shuqiang Jiang. Sim-to-real transfer via 3d feature fields for vision-and-language navigation. *arXiv preprint arXiv:2406.09798*, 2024. 2
- [51] Qiu Weichao, Zhong Fangwei, Zhang Yi, Qiao Siyuan, Xiao Zihao, Soo Tae, Kim, Wang Yizhou, and Yuille Alan. Unrealcv: Virtual worlds for computer vision. *ACM Multimedia Open Source Software Competition*, 2017. 3
- [52] Jiazhao Zhang, Kunyu Wang, Rongtao Xu, Gengze Zhou, Yicong Hong, Xiaomeng Fang, Qi Wu, Zhizheng Zhang, and He Wang. Navid: Video-based vlm plans the next step for vision-and-language navigation. *Robotics: Science and Systems*, 2024. 2, 3, 9, 10
- [53] Gengze Zhou, Yicong Hong, Zun Wang, Xin Eric Wang, and Qi Wu. Navgpt-2: Unleashing navigational reasoning capability for large vision-language models. In *Computer Vision - ECCV 2024 - 18th European Conference, Milan, Italy, September 29-October 4, 2024, Proceedings, Part VII*, volume 15065, pages 260–278, 2024. 3
- [54] Gengze Zhou, Yicong Hong, and Qi Wu. Navgpt: Explicit reasoning in vision-and-language navigation with large language models. In *Thirty-Eighth AAAI Conference on Artificial Intelligence, AAAI 2024, Thirty-Sixth Conference on Innovative Applications of Artificial Intelligence, IAAI 2024, Fourteenth Symposium on Educational Advances in Artificial Intelligence, EAAI 2014, February 20-27, 2024, Vancouver, Canada*, pages 7641–7649, 2024. 3